Available online at www.sciencedirect.com

ScienceDirect

Russian Geology and Geophysics 59 (2018) 206–215

RUSSIAN GEOLOGY AND GEOPHYSICS

www.elsevier.com/locate/rgg

Potentialities of ultrawideband GPR in low-resistivity geoenvironments

A.A. Cheremisin [a,b,*], Yu.V. Vasil'ev [b], V.V. Olenchenko [c,f], M.I. Epov [c,f], R.E. Toib [d], I.S. Shnipov [d], S.V. Shirokov [d], V.B. Boltintsev [e]

[a] *Siberian Federal University, pr. Svobodnyi 79/10, Krasnoyarsk, 660041, Russia*
[b] *Krasnoyarsk Institute of Railway Transport, Irkutsk State University of Railways, ul. Lado Ketskhoveli 89, Krasnoyarsk, 660028, Russia*
[c] *A.A. Trofimuk Institute of Petroleum Geology and Geophysics, Siberian Branch of the Russian Academy of Sciences, pr. Akademika Koptyuga 3, Novosibirsk, 630090, Russia*
[d] *GeoTekhMonitoring, ul. Baumana 3, Krasnoyarsk, 660028, Russia*
[e] *Geodizond, pr. Gagarina 14, St. Petersburg, 196211, Russia*
[f] *Novosibirsk State University, ul. Pirogova 2, Novosibirsk, 630090, Russia*

Received 20 March 2017; accepted 17 April 2017

Abstract

We assess the potentialities of ultrawideband (UWB) electromagnetic pulse sounding of low-resistivity geoenvironments using the ground-penetrating radar (GPR) system developed by us and compare the obtained results with 2D electrical resistivity tomography and standard GPR data. The research was performed in an area of Quaternary clay deposits with a resistivity of 20–50 Ohm·m. For an OKO-2 GPR antenna with a center frequency of 150 MHz, the sounding depth is 2–4 m, whereas UWB sounding provides penetration of the GPR pulse to a depth of 30–40 m. Deep UWB sounding of low-resistivity environments is possible under the following conditions: use of generators based on drift step recovery diodes (DSRDs), high matching of the UWB receiving and transmitting antennas to the environment, and an increase in the noise immunity of the recording system, in particular, due to a decrease in the intensity of air waves.

Keywords: UWB; ultrawideband GPR; electrical resistivity tomography; Quaternary clay deposits

Introduction

Recently, considerable attention has been given to engineering geological problems related to the nondestructive testing of rocks and man-caused processes. GPRs have made a definite contribution to the subsurface research in the last few decades (Lollino et al., 2015). Interest in this topic is evidenced by a large number of publications, including books (Benedetto and Pajewski, 2015; Daniels, 2004; Grinev, 2005; Jol, 2009), which deal, in particular, with studying sedimentary rocks and karst structures (Bristow and Jol, 2003), archaeological applications of GPRs (Goodman and Piro, 2013) and the detection of unexploded ordnance in the ground (Byrnes, 2008).

GPR systems differ in the configuration and characteristics of equipment manufactured by different manufacturers. However, all these systems have a common limitation on the sounding depth. The depth of GPR survey, as formulated in (Enrione et al., 2015), is within a few meters. In this work, sounding was carried out to depths of 4–5 m using a 100 MHz antenna. The depth of GPR signal penetration in a medium depends on its conductivity, as well as on the frequency to which the GPR antennas are tuned. In high-resistivity media, the sounding depth is maximal. For example, GPR using 200 MHz antennas give good results in searching for karst caverns in limestone within 10 m (Pepe et al., 2015). Even greater sounding depths (20–30 m) in fracture detection in granites can be achieved using 100 MHz antennas (Luodes et al., 2015). Low-resistivity media include Quaternary deposits with an electrical resistivity of less than 50 Ohm·m (sandy loam, loam, clay). Low subsurface resistivity is usually associated with a high content of clay particles. In this case, when using, e.g., 200 MHz antennas, the signal attenuation can be so great that it complicates the determination of the water table even at shallow depths (~3 m) (Mahmoudzadeh et al., 2012). Silty deposits also severely limit the capabilities of GPR survey (Hirsch et al., 2008).

Some approaches developed in the last decade to increase the capabilities of GPR survey are related to the expansion of

* Corresponding author.
E-mail address: aacheremisin@gmail.com (A.A. Cheremisin)

1068-7971/$ - see front matter © 2018, V.S. Sobolev IGM, Siberian Branch of the RAS. Published by Elsevier B.V. All rights reserved.
http://dx.doi.org/10.1016/j.rgg.2018.01.017

the operating frequency band and the development of so-called ultrawideband (UWB) systems (Taylor, 2012). One of the successful implementations of this approach is the development of single-pulse ultrawideband Grot-12 GPRs, which allow sounding to greater depth than conventional systems using quasi-monochromatic signals (Volkomirskaya et al., 2012). Methods for modeling the generation and propagation of UWB signals have been developed for complex conditions such as those that occur, e.g., when placing pulse probes in wells drilled in oil and gas layers (Epov et al., 2011).

In this paper, we assess the capabilities of ultrawideband electromagnetic pulse (UWB EMP) sounding of low-resistivity geological media using a GPR system that we have developed, and compare the obtained results with 2D electrical resistivity tomography (ERT) data as well as with conventional GPR data.

Ultrawideband electromagnetic pulse sounding is a variation of GPR. A nanosecond electromagnetic pulse propagating in a medium is subject to absorption, dissipation, and reflection processes, which depend on the inhomogeneity of the structure of the explored medium and its properties: dielectric permeability, electrical conductivity, and polarizability. The UWB system developed by us is based on different technical solutions (Cheremisin and Boltintsev, 2012) than Grot-12 GPRs, which, in particular, use resistively loaded receiving and transmitting antennas and spark generators of pulses.

In addition to the UWB GPR, the OKO-2 GPR was also used in this work.

Two-dimensional ERT is widely used in geophysical research. A number of studies have shown that the integration of GPR and ERT data is a successful approach to the study of complex objects such as karst systems (Carrière et al., 2013), in survey of peatland (Comas et al., 2015), and the detection of water leakage from rice fields under the impact of coal mining factors and ground fracturing (Li et al., 2015). The identification of subsurface structures by GPR sounding is also based on the results of borehole studies and survey of nearby rock outcrops. This makes it possible to improve the interpretation of the structure of sedimentary rocks, fractures, and karst formations (Fernandez et al., 2015).

This work was carried out on the basis of this approach. It is also important that ERT gives an estimate of the conductivity of the medium explored by GPR survey. We studied a medium consisting of three layers: Quaternary deposits, weathering crust and bedrock, with the uppermost layer of Quaternary deposits being low-resistivity (25–50 Ohm·m).

Study area

The research area is located on the right bank of the Ob' River, 8 km east of the Novosibirsk Akademgorodok in the area of the Klyuchi research station of the Institute of Oil and Gas Geology and Geophysics of the Siberian Branch of the Russian Academy of Sciences (INGG SB RAS), where a test site for experimental-methodological geophysical studies was established in an area adjacent to the station (Fig. 1).

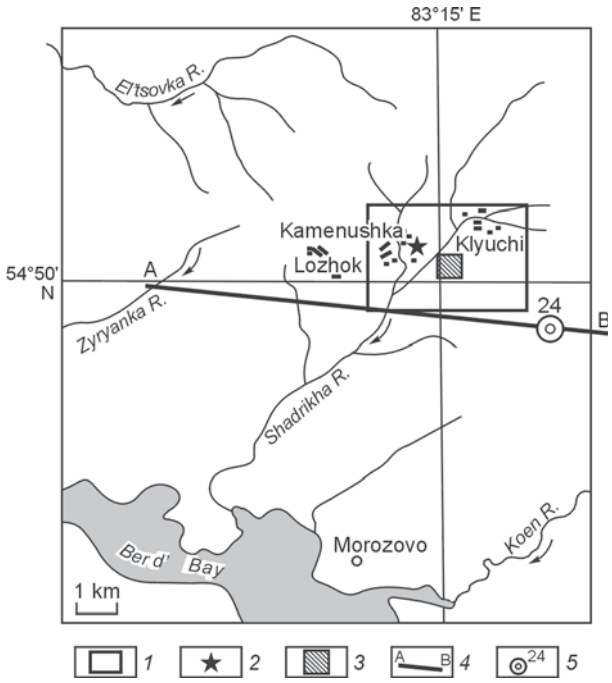

Fig. 1. Map of the study area: *1*, contour of the IPGG RAS test site; *2*, Klyuchi station; *3*, experimental-methodical UWB sounding area; *4*, geological section line; *5*, structural coring well.

The test site is located in the Shadrikha area in the basin of the small Shadrikha River. According to (Vasyutinskaya et al., 1959), the geological structure of the region consists of Yurga Formation deposits (D_3jur) represented by sandstones, siltstones, clayey and calcareous shales interbedded with limestone and mudstone. The geological section characterizing the structure of the study area is shown in Fig. 2.

Ancient weathering crust formations are widespread on the surface of the Yurga Formation. They are composed of motley-colored white kaolinite-hydromicaceous clays, which in the lower part of their section are replaced by structural residues of shales or sandstones, often preserving the structural features of the original rocks.

The depth of the top of the weathering crust from the surface varies from 0 to 106 m. The thickness of the eluvium of the weathering crust varies from 0 to 26 m. The weathering crust is overlain by Tertiary loess-like loams of the Krasnodubrovka Formation (Q_2krd). Krasnodubrovka Formation rocks occur on the Kochkovo Formation deposits (clay), Paleozoic rocks or clayey products of their weathering crust.

At the test site of the Kliuchi hospital, electrical measurements using ERT, audio-magnetotelluric sounding (AMTS), magnetic prospecting, and radiometric survey have previously been performed to study the structural and geological structure of the Shadrikha area, determine the position of the station relative to large geological structures, and express them in geophysical fields (Gornostaeva et al., 2014). The geophysical studies have shown that Quaternary clay soils (loams, clays) have a low electrical resistivity (<50 Ohm·m) and serve as a

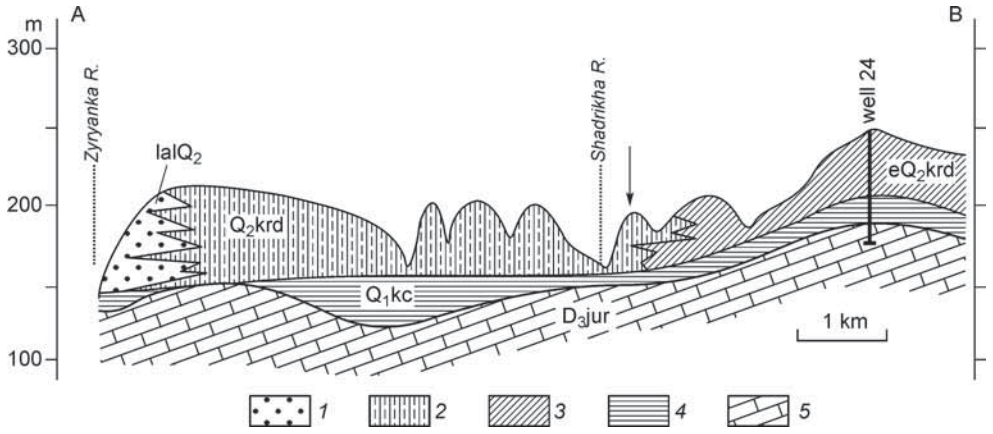

Fig. 2. Schematic geological section of the study area along the AB line (Vasyutinskaya et al., 1959): *1,* lacustrine-alluvial sands of the Krasnodubrovka Formation; *2,* interbedded lacustrine alluvial sandy loam, loam, and sand of the Krasnodubrovka Formation; *3,* cover complex of subaerial loess loams with interbedded sand, sandy loam, and clay of the Krasnodubrovka Formation; *4,* clay of the Kochkovo Formation; *5,* clayey and silty-clayey shale and limestone of the Yurga Formation. The arrow shows the UWB survey area.

conductive shield, which is an unfavorable factor for the use of conventional GPR, e.g., to determine the position of the top of hard rock. Experimental studies of the capabilities UWB GPR in sounding low-resistivity geological environments have been conducted within one of the selected zones with a thick (up to 25 m) low-resistivity sedimentary cover with a structure close to horizontally layered.

Methods of research

Electrical resistivity tomography is a modern modification of the vertical electrical sounding method (Balkov et al., 2012; Loke, 2009) and belongs to the group of resistivity methods based on Ohm's law.

In ERT sounding, we used a Skala-48 system (Balkov et al., 2012). The system is a single-channel electro-prospecting station switching the connection of 48 electrodes. The distance between the electrodes on a standard cable is 5 m.

Preliminary studies within the study area site showed that the previously used ERT array with maximum separations of the AB transmission line of up to 235 m did not provide sufficient sounding depth to unambiguously determine the position of top of the Paleozoic basement in the section.

The structure of the section was studies using a sounding cable with an interelectrode spacing of 10 m and a maximum AB spacing of up to 470 m. In soundings, we used three electrode connection configurations corresponding to the Schlumberger array and the forward and reverse three-electrode (pole-dipole) arrays. This combination of these arrays gives the best results in data inversion than each of the arrays separately (Balkov et al., 2012; Bobachev and Gorbunov, 2005; Dahlin and Zhou, 2004; Szalai and Szarka, 2008).

In the measurements, the current in the transmission line was varied between 150–450 mA and the difference across the potential electrodes was 1.7–180 mV. With a statistical integration of five pulses, the mean square error of measurements usually did not exceed 1%. Single measurements with an error of more than 1% were discarded. The total number of measurements was 520 for the Schlumberger array and 792 for each of the pole-dipole configurations.

The set of measured apparent resistivities was used later to solve the inverse problem of determining the distribution of the true resistivity along the section (2D data inversion). This problem was carried out using the Res2Dinv software version 3.56 (Loke, 2009) under standard constraints. For inversion, we used the so-called bounded-smooth domain robust inversion (Loke, 2009) based on minimizing the sum of the squares of the difference between the measured and calculated apparent resistances. The iterative procedure was interrupted at a less than 5% convergence of the standard deviation along the section between iterations. At an interelectrode spacing of 10 m, a geoelectric section along the profile was constructed to a depth of up to 85 m.

GPR survey using an OKO-2 equipment. Along the ERT profile, we carried out GPR sounding using an OKO-2 GPR (Logis, Russia) with an antenna unit with a center frequency of 150 MHz. This frequency provides a satisfactory resolution in depth, about a dozen centimeters. The choice of an antenna with a frequency of 100 to 250 MHz is a common practice of compromise between penetration depth and depth resolution (Carrière et al., 2013; Comas et al., 2015), which is used for exploration in sedimentary rock (Bristow and Jol, 2003), including limestone (Pepe et al., 2015), as well as hard rock, e.g., granite (Luodes et al., 2015). The total length of the section (100 m) was measured by a tape-measure, and distance along the profile by the displacement sensor of the OKO-2 GPR; the signal recording time was 400 ns; the interval along the profile (the distance between neighboring equidistant points at which the signal was recorded) was 0.05 m; the integration was 128 times to improve the signal-to-noise ratio.

For time-depth conversion of both OKO-2 and UWB measurements, we used the same relative dielectric permeability of 14, which corresponds to a signal propagation speed of

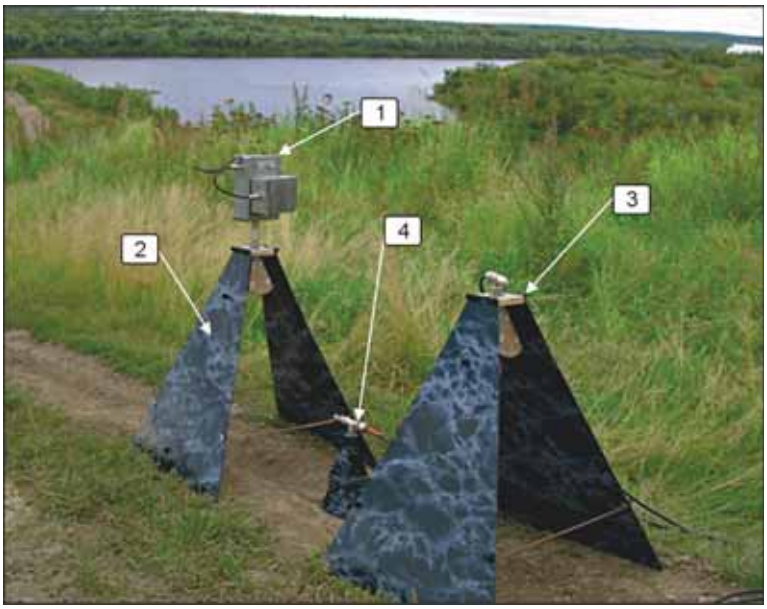

Fig. 3. General view of the receiving and transmitting equipment for UWB EMP sounding: 1, electromagnetic pulse generator based on DSRDs; 2, UWB bi-leaf microstrip transmitting antenna; 3, receiving antenna similar to 2; 4, UWB monopole receiving antenna.

0.080 m/ns. This speed is the result of averaging the measurement data gained from diffraction hyperbolas from point objects in the medium for both OKO-2 and the UWB data. This speed is characteristic of the media studied and is similar to that obtained in our previous work.

Processing of the OKO-2 GPR data was carried out using the GeoScan32 software (Logis, Russia) (GeoScan32..., 2013) or the Georadar-Expert[1] software and included procedures such as subtraction of the average for each individual record, signal amplitude amplification depending on the depth for each individual record of the average amplitude envelope to compensate for signal attenuation, and frequency bandpass filtering.

The boundaries of the layers were traced along extended wave patterns in radargrams, and local objects were identified by the presence of a diffracted wave (diffraction hyperbole).

UWB EMP sounding. UWB GPR sounding was carried out in the same interval of the ERT profile and the OKO-2 GPR profile.

The hardware part of the UWB system sounding used in this work consisted of special generators of electromagnetic pulses and ultrawideband antenna systems (Fig. 3).

The UWB radar systems designed for sounding materials include devices based on the generation and transmission of short electromagnetic pulses. In practice, two most important wideband criteria are widely used. One of these is the ratio of the operating frequency bandwidth to the center (or middle) band frequency, which for wideband systems should be greater than 20–25%. Another criterion defines the absolute band of operating frequencies, which should be more than 500–700 MHz wide (Taylor, 2012).

Systems using pulses less than 1.5 ns meet both criteria. This provides high spatial resolution in GPR sounding of natural media and structural materials to a shallow depth, e.g., in examining asphalt road surfaces or inspection of reinforcing bars in concrete blocks, in sounding through walls, in mine detection, and medical examination (Bugaev et al., 2010).

Most GPRs used in engineering geology and geophysics for sounding to a depth of more than 1 m have center frequencies in the range of less than 500–700 MHz and are designed so that the ratio of the operating frequency bandwidth to the center frequency is approximately 100% (Annan, 2009; Neto and Medeiros, 2006). Formally, according to the relative frequency bandwidth criterion, they can be classified as UWB systems. However, they do not satisfy the absolute bandwidth criterion.

The spatial resolution of GPRs for subsurface sounding is proportional to the center frequency of the signal. The resolution is higher the higher the frequency. However, high-frequency signals attenuate more rapidly, and to increase the sounding depth, the signal frequency has to be reduced. Therefore, for GPR applications, it is required to find a compromise between spatial resolution and depth, and this is achieved by selecting the appropriate frequency for a particular problem. This is one of the reasons why practical GPR systems are equipped with a whole set of antennas having different center frequencies.

The well-known SIR-3000 GPRs produced by Geophysical Survey Inc. in the US are equipped with antennas with center frequencies of 2.6, 1.6, and 0.9 GHz for the high-frequency region and 400, 270, 200, 100, and 16–80 MHz (SIR site) for the low-frequency region. The GPRs produced by Logis-Geotech in Russia have antenna units with center frequencies of 700, 400, 250, 150, 90, and 50 MHz (Geotech site) for the low-frequency region. The same is true for the Mala Ground

[1] Georadar-Expert. http://www.georadar-expert.ru.

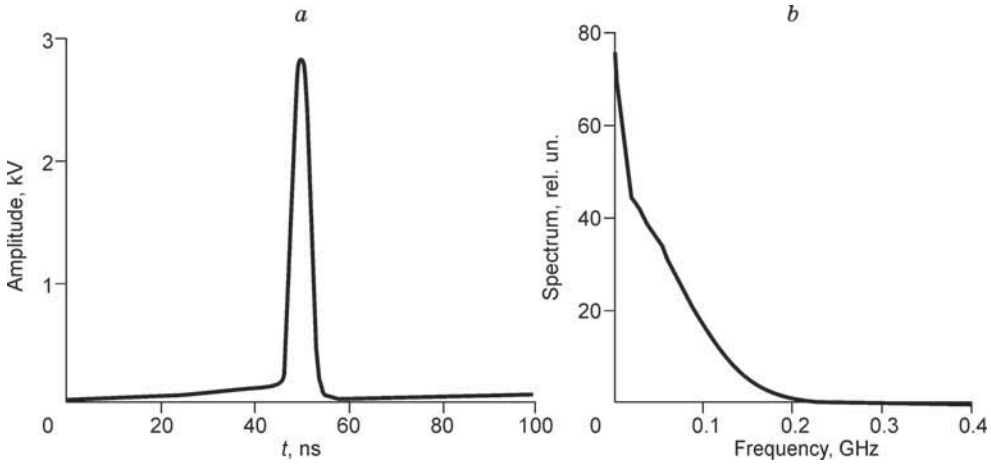

Fig. 4. Pulse of the DSRD generator used in this study for UWB GPR (*a*) and the spectrum of this pulse (*b*).

Explorer (Mala GeoScience), Pulse Ekko Pro, and Noggin (Sensors & Software Inc.), and other GPRs.[2]

The UWB GPR system used in our work is based on a somewhat different principle (Cheremisin and Boltintsev, 2012). The most important difference is that measurements at all frequencies use the same wideband antennas, which are well matched to the environment and operate at 1–700 MHz. The ratio of the operating frequency bandwidth to the center frequency for these antennas is 2. In terms of this parameter, our system has a wider frequency band than conventional systems. Moreover, it satisfies both mentioned wideband criteria.

For wideband GPRs of this type, there is no need to find a compromise between depth and spatial resolution; i.e., there is no need to change antennas and pulse generators to increase the sounding depth as this occurs automatically. Reflected signals from shallow depths contain high frequencies, and with increasing depth, high frequencies are attenuated and the signal becomes low-frequency. An approach based on information entropy criteria (Korolev, 2011; Kullback and Leibler, 1951; Shannon, 1963) has also been developed to solve the inverse sounding problem—the identification of the subsurface structure from GPR measurement data at a single spatial point. In principle, considering the set of features that distinguish this method from conventional GPR methods, it is a separate method—the ultrawideband electromagnetic pulse (UWB EMP) subsurface sounding method. This method has found wide application in geology and the building industry (Bezrodnyi et al., 2010; Boltintsev et al., 2006).

Wideband sounding of the subsurface requires nanosecond electromagnetic pulse generators with stable amplitude-frequency characteristics. Generators based on superfast drift step recovery diodes (DSRDs), which can generate nanosecond and picosecond pulses, have proved to be effective for this purpose (Grekhov et al., 1983). It is known that the peak current amplitude in such devices can reach 800 A (Grekhov and Mesyats, 2005). A whole range of powerful generators having stable characteristics has been specifically designed for GPR applications. In general, we have used a set of nanosecond pulse generators produced by the DSRD technology specifically for GPR studies and having pulse edges roughly equal to 0.5, 1, 3 ns at a duration of 3 to 10 ns, a voltage pulse peak amplitude of 1, 3, 4.77, 6.3, 9.87 kV, and a peak current amplitude of 20 to 120 A. Increasing the generator power is the simplest and most effective way to increase the depth of GPR surveys.

In this work, we used a DSRD generator (Fig. 3(1)) with a voltage pulse peak amplitude of ~3 kV, a duration of ~8 ns, and a peak current amplitude of 40 A. The view of a DSRD generator pulse on the TRM 8105 oscilloscope screen (with an operating frequency bandwidth $\Delta f \sim 16$ GHz) measured with a BARTH attenuator, which is a resistance of 50 Ohm in a frequency band $\Delta f \sim 26$ GHz is shown in Fig. 4, together with the amplitude of the Fourier spectrum of this pulse, which increases toward low frequencies.

One of the major problems in developing GPR antennas is the impedance matching of the antenna to the subsurface. In this work, two types of antennas were used: a UWB bi-leaf microstrip antenna (Fig. 3 (2, 3)) and an UWB monopole antenna (Fig. 3 (4)). Both antennas are well matched to the environment over a wide frequency range (Fig. 5). The voltage standing wave ratio k_ω was measured with an OBZOR-103 vector analyzer (Tekhnicheskii Tsentr, Russia) (OBZOR-103) using an 50 Ohm measurement channel. The results are shown for the range from 1 to 750 MHz. The measurement error varies from 2.5% for $k_\omega = 1$ to 4.5% for $k_\omega = 1.85$. The antennas were placed on dry sand or gravel-pebble ground. As can be seen, $k_\omega < 1.85$ for the microstrip antenna in the frequency band of 0.3–700 MHz and for the monopole antenna in the frequency band of 0.3–650 MHz. With this matching level, energy from the generator is transferred to the antenna without significant losses.

In addition to the closeness of the voltage standing wave ratio to unity, good matching to the environment implies that

[2] Antenna Units. http://www.geotechru.com/market/geophysical_equipment/ground_ penetrating_radar_gpr/antenna_units/

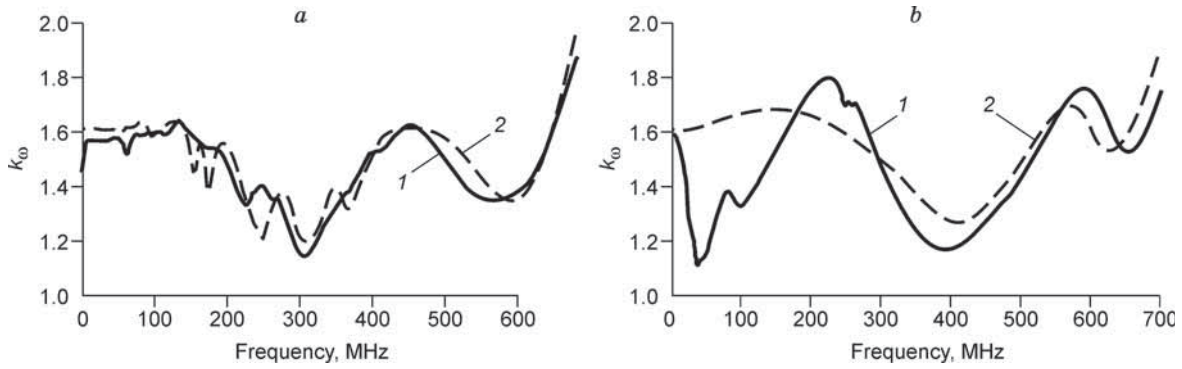

Fig. 5. Voltage standing wave voltage ratio k_ω versus frequency for different media. *a,* Bi-leaf microstrip antenna; *b*, monopole antenna. *1,* antennas on pebble-gravel ground; *2,* on sand.

the electromagnetic pulse energy is transferred to the underlying environment and does not propagate in the air, producing heavy synchronous interference upon reflection from obstacles located on the ground. The hardware provides an increased noise immunity for the receiving and recording unit under field conditions. These questions will be discussed below. Signals were recorded using a LeCroy WavePro7100A digital axes oscillograph with a bandwidth $\Delta f \sim 1$ GHz and a 10 GHz sampling band. This antenna configuration is capable of UWB sounding to depths of 40–80 meters, depending on the type of media studied.

UWB sounding data were processed similarly to GPR OKO-2 data using the GeoScan32 software and high-quality radargrams were obtained. To achieve the objectives set out in this study, we did without using the above-mentioned special techniques we have developed to process UWB sounding data.

Results

A geoelectric section to a depth of ~85 m was constructed from the ERT data (Fig. 6). The upper part of the section to a depth of 10–20 m has a low (25–40 Ohm·m) resistivity. These values are typical of loam and sandy loam in the study area. A feature of the section is an increase in the thickness of the upper conductive layer from 10 to 20 m along the strike of the profile. The underlain by rocks with a resistivity of 70–100 Ohm·m are interpreted as weathered shales. From a depth of about 65 m, the top of a high-resistivity base with a resistivity of 160–300 Ohm·m is identified in the section. The resistivity increases to 800–2500 Ohm·m with depth.

Figure 7 shows an OKO-2 radargram along the ERT profile obtained using an antenna unit with a center frequency of 150 MHz. The depth scale in the radargram is constructed for an average dielectric permeability of the section ε = 14. Reflectors in the upper part of the section to a depth of 4 m are identified from extended wave patterns. In the same subsurface layer, diffraction hyperbolas from local objects are identified. At times later than 100 ns (depths greater than 4 m), reflections from objects in the air clearly detected based on characteristic diffraction hyperbolas; visible reflecting boundaries in the section are not observed.

A feature of GPRs is the presence of a strong direct air wave from the transmitter to the receiver without penetration into the explored medium. This wave is pronounced in

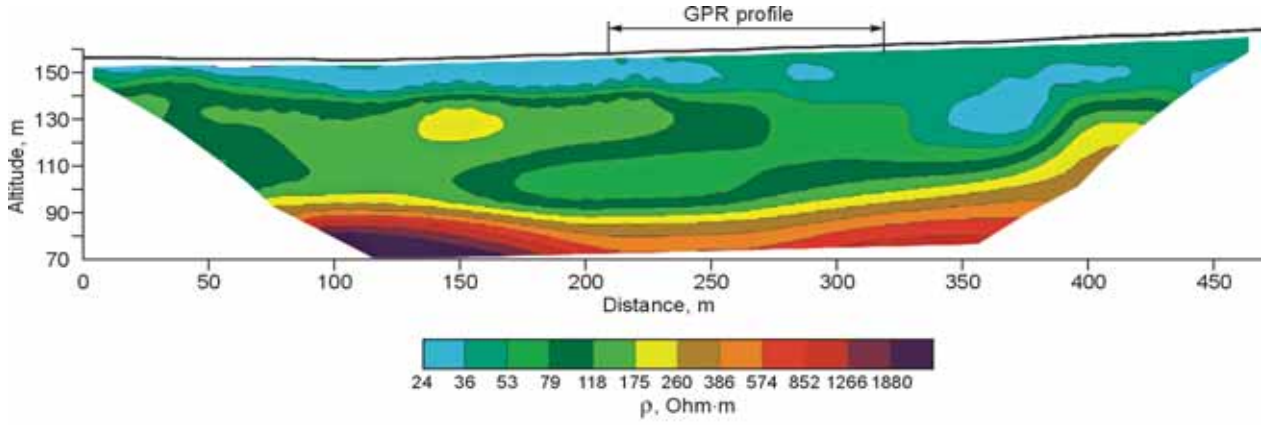

Fig. 6. Geoelectric section according to electrical resistivity tomography data. The part of the profile where GPR investigations were carried out simultaneously is indicated.

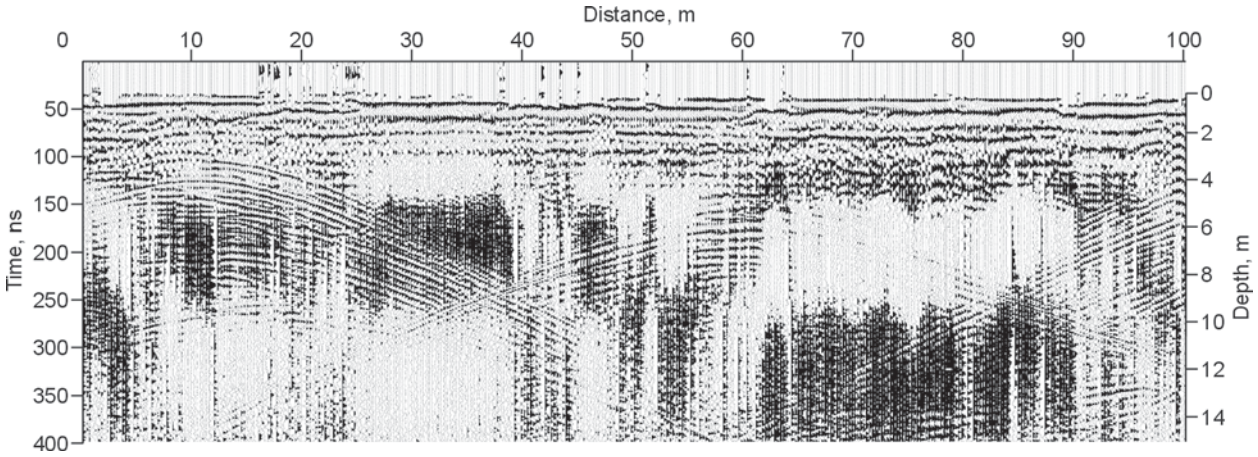

Fig. 7. OKO-2 GPR record along the electrical resistivity tomography profile. 150 MHz antenna unit; the average relative dielectric permeability ε = 14.

radargrams at the very early times. Basically it is interference. In the same time range, a surface wave is detected, whose amplitude depends on the distance from the source and the lateral homogeneity of the top layer. These waves are easily identified in GPR studies with a variable base (Vladov and Starovoitov, 2004).

In the UWB system used, the direct air wave is highly attenuated. To demonstrate this effect, we performed a special experiment involving measurements with a variable distance between the transmitting and receiving antennas. Figure 8 shows the time section obtained using the UWB bi-leaf antenna which was shifted with step of 2 m from the position of the transmitting antenna of the same type to a distance of 20 m. The measurements were made along the GPR profile in its initial part. The signal attenuation for each measurement line with increasing distance between the antennas as well as with the attenuation with time was compensated by the automatic amplification control included in the software used.

As we see, the results of the studies with a variable distance between the transmitting and receiving antennas indicate the virtual absence of a direct air wave when using the UWB system. In this case, according to estimates, the amplitude of the direct air wave is approximately two orders of magnitude weaker than the wave propagating horizontally along the ground surface. This, together with the closeness of the voltage standing wave ratio to unity (Fig. 5), indicates that the antennas are well matched to the environment. The energy

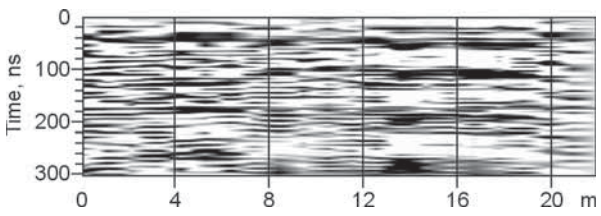

Fig. 8. Time section with a sweep length of up to 300 ns obtained by the UWB system with increasing distance between the receiving and transmitting antennas.

supplied to the antenna is transferred into the ground and does not propagate in the air.

Moreover, the resulting profile does not have inclined travel-time curves of direct electromagnetic (air and surface) waves, which is not typical of standard GPR records with increasing distance between the receiving antenna and the transmitting antenna above a layered section. The fact is that in most of the transmission antennas and antenna units of domestic and foreign GPRs developed to date, recording is triggered by a clock signal. The dominant wave fronts that are usually observed are a direct air eave and then a direct surface wave (Bristow and Jol, 2003; Grinev, 2005). The power of the air wave is usually sufficient for its detection at a distance of 10 m (Neto and Medeiros, 2006), whereas a feature of the developed measurement technique using the UWB system is the absence of direct (fiber) synchronization of the start of recording of GPR signals by a generator pulse. Recording of the signal (response) begins when its value exceeds a predetermined threshold. Since in the operation of the UWB system, we do not observe a direct air wave that could arrive at the receiving antennas earlier than other electromagnetic waves, the start of recording in the UWB system is measured from the arrival of the direct wave propagating along the ground surface.

The absence of the synchronization channel allows the depth GPR survey to be increased due to signal integration. Special experiments conducted in the development of the UWB system showed that the synchronization channel is the source of structural noise (similar to the signal) which is very substantial in sounding at great depths. Signal integration becomes inefficient in this case.

Comparison of UWB EMP and ERT data

A radargram based on UWB sounding data and a fragment of the geoelectric section constructed from ERT data are shown in Fig. 9. Comparison shows general similarity between the radargram and the fragment of the geoelectric section.

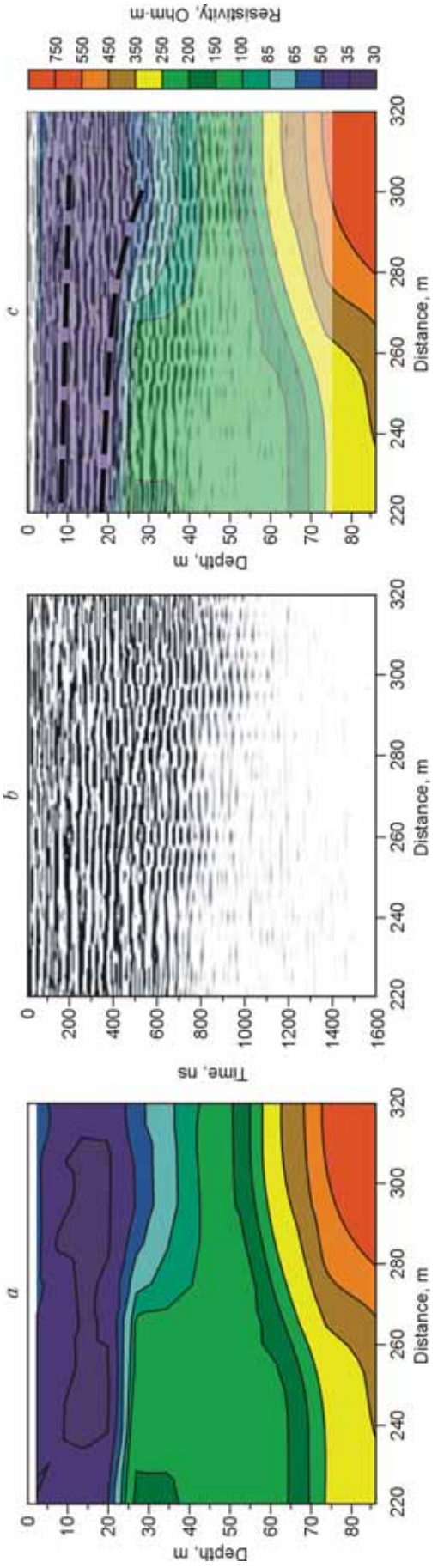

Fig. 9. Geoelectric section based on ERT data (*a*), UWB EMP radargram (*b*), and the combined section (*c*).

The upper part of geoelectric section (Fig. 9*a*) to a depth of 20 to 30 m has a resistivity of 30–50 Ohm·m (loam). The radargram (Fig. 9*b*) clearly shows the layered structure of the subsurface. Wave patterns indicate the presence of reflectors at times 200 and 400 ns.

Comparison of the radargram and the geoelectric section (Fig. 9*c*) leads to the conclusion that the reflector at a time of 400 ns corresponds to the geoelectric boundary of rock units with resistivities of 30–50 and 100–250 Ohm·m at a depth of 20–30 m. The low-resistivity rock unit is characterized by a high-amplitude signal. At times larger than 600–800 ns, the amplitude-frequency pattern of the radargram changes, which correspond to the change in the geoelectric complexes in the resistivity profile.

Signals from the UWB antenna are clearly distinguished from noise at times up to 750 ns for the sounding points at the left edge of the profile and at 1100 ns for points in the right part of the profile (Fig. 10). This corresponds to the penetration of the GPR pulse into the weathered layer to a depth of 30 and 44 m, respectively. In this case, according to the ERT data, the conductivity of the top of the sediments, which largely determines the attenuation of GPR signals is much higher at the beginning of the profile than at the end of the profile.

Conclusions

The capabilities UWB GPR in sounding low-resistivity geological media were experimentally assessed and compared with classical GPR and ERT data.

According to the ERT data, Quaternary clay rocks (loam, clay) of the upper part of the section to a depth of 20 to 30 m have a low resistivity of 20–50 Ohm·m. The low-resistivity upper layer is an unfavorable factor for the traditional GPR that limits the survey depth to several meters (2–4 m) using an antenna unit with a center frequency of 150 MHz. In sounding using the OKO-2 GPR, the noise region starts at 150 ns, whereas in measurements using the UWB, at 800–1000 ns.

Unlike the dipole antennas typically used in domestic and foreign GPR systems, the UWB system uses a monopole antenna and a bi-leaf antenna, in which the direct air wave is strongly suppressed, as shown by the field experiment. Experimental studies with a variable distance between receiving and transmitting antennas have shown that the electromagnetic waves propagating in the air are much weaker than surface waves. This, along with the closeness of the voltage standing wave ratio to unity, confirms the good matching of the antennas to the environment and the high noise immunity of the receiving-recording unit as a whole. The electromagnetic pulse energy is transferred into the subsurface and does not spread in the air, producing heavy interference.

Thus, the depth of UWB GPR sounding of low-resistivity environments can be increased by using special powerful electromagnetic pulse generators based on drift step recovery diodes, by good matching of the receiving and transmitting

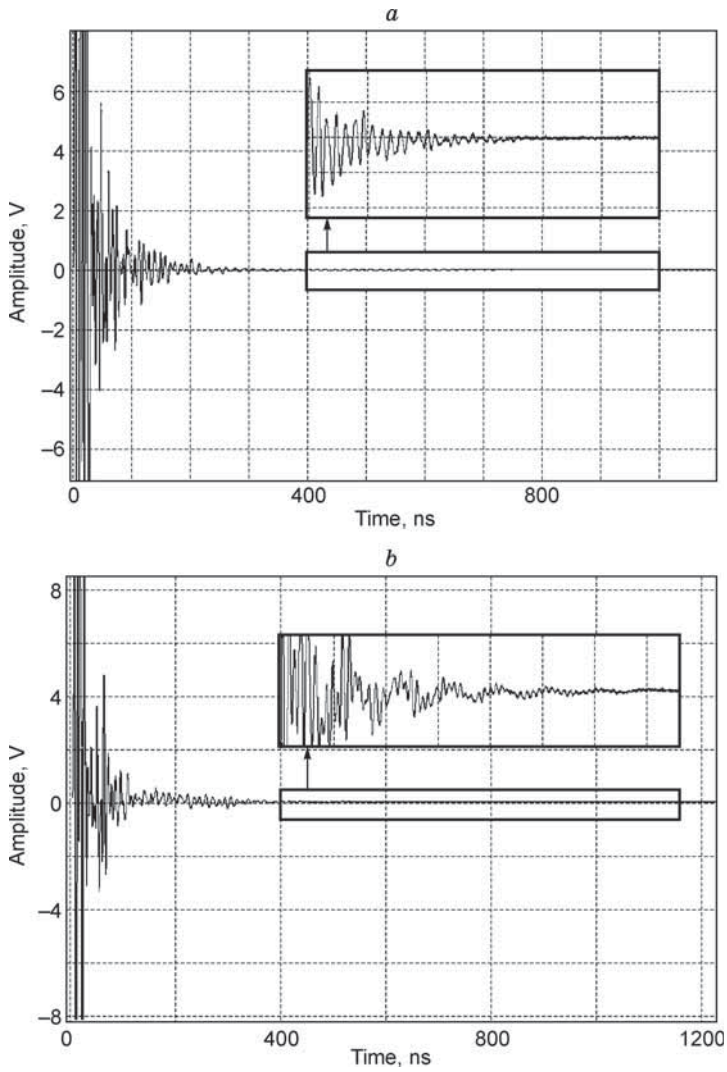

Fig. 10. UWB signal received by the UWB bi-leaf antenna at the beginning (*a*) and end (*b*) of the profile.

antennas to the environment, and by improving the noise immunity of the recording system as a whole, in particular, by reducing the intensity of the air waves.

References

Annan, A.P., 2009. Electromagnetic principles of ground penetrating radar, in Jol, H.M. (Ed.), Ground Penetrating Radar: Theory and Applications. Elsevier Science, Oxford, UK.

Balkov, E.V., Panin, G.L., Manshtein, Yu.A., Manshtein, A.K., Beloborodov, V.A., 2012. Electrical resistivity tomography: equipment, technique, and application. Geofizika, No. 6, 54–63.

Benedetto, A., Pajewski, L. (Eds.), 2015. Civil Engineering Applications of Ground Penetrating Radar. Springer Transactions in Civil and Environmental Engineering. Springer, Switzerland.

Bezrodnyi, K.P., Boltintsev, V.B., Il'yakhin, V.N., Andrianov, S.V., 2010. Monitoring of the underground space ahead of the mining face by ultrawideband pulse electromagnetic sounding: Research of the case study of the construction of tunnels in Sochi. Zhililshchnoe Stroitel'stvo, No. 12, 40–44.

Bobachev, A.A., Gorbunov, A.A., 2005. Two-dimensional electrical resistivity and induced polarization sounding: equipment, technique, and software. Razvedka i Okhrana Nedr, No. 12, 52–54.

Boltintsev, V.B., Il'yakhin, V.N., Cheremisin, A.A., Bezrodnyi, K.P., Nagornyi, S.Ya., 2006. UWB electromagnetic pulse sounding in geological engineering surveys. Inzhenernaya Geologiya, No. 2, 72–76.

Bristow, C.S., Jol, H.M., (Eds.), 2003. Ground penetrating radar in sediments: advice on data collection, basic processing and interpretation, a good practice guide. Geol. Soc. London Spec. Publ. 211, 9–27.

Bugaev, A.S., Ivashova, S.I., Immoreeva, I.Ya., (Eds.), 2010. Bioradar [in Russian]. Izd. MGTU, Moscow.

Byrnes, J. (Ed.), 2008. Unexploded Ordnance Detection and Mitigation. (NATO Science for Peace and Security Series B_ Physics and Biophysics). Springer, Dordrecht, Netherlands,.

Carrière, S.D., Chalikakis, K., Sénéchal, G., Danquigny, C., Emblanch, C., 2013. Combining electrical resistivity tomography and ground penetrating radar to study geological structuring of karst unsaturated zone. J. Appl. Geophys. 94, 31–41, http://dx.doi.org/10.1016/j.jappgeo.2013.03.014.

Comas, X., Terry, N., Slater, L., Warren, M., Kolka, R., Kristijono, A., Sudiana, N., Nurjaman, D., and Darusman, T., 2015. Imaging tropical peatlands in Indonesia using ground penetrating radar (GPR) and electrical resistivity imaging (ERI): implications for carbon stock estimates and peat soil characterization. Biogeosci. Discuss. 12, 191–229, www.biogeosciences-discuss.net/12/191/2015/, doi:10.5194/bgd-12-191-2015.

Cheremisin, A.A., Boltintsev, V.B., 2012. Wideband GPR. Izv. Vuzov. Fizika 55 (8/2), 12–19.

Dahlin, T., Zhou, B., 2004. A numerical comparison of 2D resistivity imaging with ten electrode arrays. Geophys. Prospect. 52, 379–398.

Daniels, D.J. (Ed.), 2004. Ground Penetrating Radar. The Institution of Electrical Engineers, London, United Kingdom.

Enrione, R., Cocchi, S., Naldi, M., 2015. The combined use of different near surface geophysics techniques and geotechnical analysis in two case histories for the advanced design of underground works in urban environment: Rome metro B and Torino-Ceres railway, in: Geol. Soc. Terr. Applied Geology for Major Engineering Projects. Springer, Switzerland, Vol. 6, pp. 1045–1048.

Epov, M.I., Mironov, V.L., Muzalevskii, K.V., 2011. Ultrawideband Electromagnetic Sounding of Oil and Gas Reservoirs [in Russian]. Izd. SO RAN, Novosibirsk.

Fernandez, Jr., A.L., Medeiros, W.E., Bezerra, F.H.R., Oliveira, Jr., J.G., Cazarin, C.L., 2015. GPR investigation of karst guided by comparison with outcrop and unmanned aerial vehicle imagery. J. Appl. Geophys. 112, 268–278, doi: 10.1016/j.jappgeo.2014.11.017.

GeoScan32. Illustrated User's Manual, 2013. LOGIS, Ramenskoe.

Goodman, D., Piro, S., 2013. GPR Remote Sounding in Archaeology. Springer, Berlin.

Gornostaeva, E.S., Olenchenko, V.V., Potapov, V.V., 2014. Structure of the Shadrikha fault (right bank of the Ob' River region) according to audiomagnetotelluric sounding, in: Proc. Int. Sci. Conf. "Subsoil Use. Mining. Directions and Technologies of Exploration and Development of Mineral Resources. Geoecology" [in Russian]. Novosibirsk, pp. 32–35.

Grekhov, I.V., Mesyats, G.A., 2005. Nanosecond semiconductor diodes for high-current interruption. UFN 175 (7), 735–744.

Grekhov, I.V., Efanov, V.M., Kardo-Sysoev, A.F., Shenderei, S.V., 1983. Formation of high-voltage nanosecond voltage drops across semiconductor diodes with the drift voltage recovery mechanism. Pis'ma v Zhurnal Tekhnicheskoi Fiziki 9 (7), 435–439.

Grinev, A.Yu. (Ed.), 2005. Problems of Ground Penetrating Radar [in Russian]. Radiotekhnika, Moscow.

Hirsch, M., Bentley, L. R., Dietrich, P., 2008. A comparison of electrical resistivity, ground penetrating radar and seismic refraction results at a river terrace site. J. Environ. Engin. Geophys. 13 (4), 325–333.

Jol, H.M. (Ed.), 2009. Ground Penetrating Radar: Theory and Applications. Elsevier Science, Oxford, UK.

Korolev, V.Yu., 2011. Probabilistic Statistical Methods for the Decomposition of the Volatility of Chaotic Processes [in Russian]. Izd. Mosk. Gos. Univ., Moscow.

Kullback, S., Leibler, R.A., 1951. On information and sufficiency. The Annals of Mathematical Statistics 22 (1), 79–86.

Li, X., Hu, Z., Li, S., Cai, Y., 2015. Anomalies of mountainous mining paddy in western China. Soil Tillage Res. 145, 10–19, https://doi.org/10.1016/j.still.2014.07.021.

Loke, M.H., 2009. Electrical imaging surveys for environmental and engineering studies. A practical guide to 2-D and 3-D surveys, RES2DINV Manual. IRIS Instruments.

Lollino, G., Manconi, A., Guzzetti, F., Culshaw, M., Bobrowsky, P., Luino, F. (Eds.), 2015. Engineering Geology for Society and Territory. Urban Geology, Sustainable Planning and Landscape Exploitation. Springer, Switzerland, Vol. 5.

Luodes, H., Sutinen, H., Härmä, P., Pirinen, H., Selonen, O., 2015. Assessment of potential natural stone deposits, in: Lollino, G., Manconi, A., Guzzetti, F., Culshaw, M., Bobrowsky, P., Luino, F. (Eds.), Engineering Geology for Society and Territory. Urban Geology, Sustainable Planning and Landscape Exploitation. Springer, Switzerland, Vol. 5, pp. 243–246.

Mahmoudzadeh, M.R., Francés, A.P., Lubczynski, M., Lambot, S., 2012. Using ground penetrating radar to investigate the water table depth in weathered granites—Sardon case study, Spain. J. Appl. Geoph.79, 17–26, http://dx.doi.org/10.1016/j.jappgeo.2011.12.009.

Neto, P.X., Medeiros, W.E., 2006. A practical approach to correct attenuation effects in GPR data. J. Appl. Geophys. 59, 140–151.

OBZOR-103. Meter of Complex Transmission Coefficients. http://www.jais.ru/obzor103.html.

Pepe, P., Martimucci, V., Parise, M., 2015. Geological and geophysical techniques for the identification of subterranean cavities, in: Lollino, G., Manconi, A., Guzzetti, F., Culshaw, M., Bobrowsky, P., Luino, F. (Eds.), Engineering Geology for Society and Territory. Urban Geology, Sustainable Planning and Landscape Exploitation. Springer, Switzerland, Vol. 5, pp. 483–487.

Shannon, C.E., 1963. A mathematical theory of communication, in: Works on Information Theory and Cybernetics [Russian translation]. Izd. Inostrannoi Literatury, Moscow, pp. 243–332.

SIR Site: Ground Penetrating Radar Data Acquisition Unit—SIR-3000 – GSSI. http://www.geophysical.com/sir3000.htm.

Szalai, S., Szarka, L., 2008. On the classification of surface geoelectric arrays. Geophys. Prosp. 56 (2), 159–175.

Taylor, J.D. (Ed.), 2012. Ultrawideband Radar: Applications and Design. CRC Press, Boca Raton–London–New York.

Vasyutinskaya, T.F., Kutolin, V.A., Mikhailovskii, D.V., et al., 1959. Geological structure and minerals, in: Data on a 1:200,000 State Geological Map of the USSR. Sheet N-44-XII [in Russian]. TGF, Novosibirsk.

Vladov, M.L., Starovoitov, A.V., 2004. An Introduction to Ground Penetrating Radar [in Russian]. Izd. Mosk. Univ., Moscow.

Volkomirskaya, L.B., Gulevich, O.A., Varenkov, V.V., Reznikov, A.E., Sakhterov, V.I., 2012. Modern GROT GPR for environmental monitoring. Ekologicheskie Sistemy i Pribory, No. 5, 1–3.

Editorial responsibility: A.D. Duchkov